Electron Hopping Transport in Two-Dimensional Semiconductor - Zinc Oxide Nanoflakes

Dunliang Jian,[1†] Yen-Fu Lin,[2†] Jiangpang Zhai,[1] Irene Ling Li,[1] Shulin Wang,[3] Ping Hua,[1,4] Jian-Jhong Lai,[5] Ming-Ming Ku,[5] Wen-Bin Jian,[5,a] Shuangchen Ruan,[1,a] and Zikang Tang[6]

[1]*Shenzhen Key Lab of Laser Engineering, Key Lab of Advanced Optical Precision Manufacturing Technology of Guangdong Higher Education Institutes, and College of Optoelectronic Engineering, Shenzhen University, Shenzhen , Guangdong 518060, China*

[2]*Department of Physics, National Chung Hsing University, Taichuung, Taiwan, ROC*

[3]*College of Energy and Power Engineering, University of Shanghai for Science and Technology, Shanghai 200093, China*

[4]*Optoelectronics Research Centre (ORC), University of Southampton, Southampton, United Kingdom*

[5]*Department of Electrophysics, National Chiao Tung University, 1001 Ta Hsueh Road, Hsinchu, Taiwan, ROC*

[6]*Department of Physics, The Hong Kong University of Science & Technology, Clear Water Bay, Kowloon, Hong Kong*

[a)] Electronic mail: wbjian@mail.nctu.edu.tw; *scruan@szu.edu.cn*.

† The authors contributed equally to this work.

ABSTRACT

The sequential hydrothermal process is used to synthesize ZnO nanostructures on Si substrates. The synthesized ZnO nanostructures are inspected by scanning electron microscope and transmission electron microscope. They present a morphology of two-dimensional structures, named nanoflakes. The ZnO nanoflakes have a thickness of tens of nanometers. The energy dispersive x-ray spectrum reveals their compositions of only Zn and O elements. In addition, its crystalline structures are investigated by high-resolution transmission electron microscope. The nanoflakes are then dispersed for another morphology measurement using atomic force microscope and their average thickness is determined. The dispersed nanoflakes are contacted with metal electrodes for electron transport measurements. Through the analysis of electrical and temperature dependences of resistivity, it is confirmed that the electron transport in ZnO nanoflakes agree well with the theory of Mott's two-dimensional variable range hopping. The nature of two-dimensional electron system in ZnO nanoflakes points to the application of this two-dimensional semiconductor as new channel materials for electronic devices.

THE MAINTEXT

ZnO is a hot material and has been studied since 1930s [1]. It is ever in the list of polar crystals for studying the polaron's playing role in electron transport [2]. This material is explored due to its transparency in the visible light bandwidth whereas it is conductive because of defects. This transparent, conductive metal oxide is usually accepted as essential substances for optoelectronics. The defects in ZnO is an important while controversial issue. Oxygen vacancies, zinc interstitials, and hydrogen doping [3] are usually regarded as native defects of ZnO [4,5]. The interaction between native defects is intensely discussed [6]. ZnO is easily *n*-type doped whereas *p*-type doping is continuously attempted, as well, for full utilization of this material in electronic devices [7]. On the other hand, its optical properties are thoroughly explored since it has large exciton binding energy for room-temperature lasing [8]. ZnO is of wurtzite structure at ambient conditions and many facile preparation methods, such as chemical vapor deposition, pulsed laser deposition, molecular beam epitaxy, thermal evaporation and hydrothermal approaches, have been implemented in crystal growth and nanostructure formation [1,5]. Recently, it draws much attention in the synthesis of controlled-shape nanoparticles and nanowires [9,10]. The application of ZnO in nanoelectronics, piezotronics and nanoenergy grows rapidly [11-13].

Since the successful mechanical exfoliation of single-layer graphene by Novoselov and Geim [14], the exploration of two-dimensional (2D) electron system, especially in the 2D semiconductors, becomes practical. The 2D semiconductors can be either exfoliated mechanically or chemically from layer materials such as transition metal dichalcogenides. Alternatively, the 2D materials can be formed and deposited by chemical vapor or pulsed laser depositions [15]. In fact, electron transport needs to be investigated to check whether it in the materials presents 2D nature or not. For weak and strong disordered systems, the electron system manifests itself as weak localization and Mott's 2D variable range hopping transport, respectively, in temperature dependent resistivity [16]. In certain conditions of strong electron-electron interactions, a metallic state as well as a transition from metal to insulator are observable in 2D materials as well [16]. It is learned that the material reveals 2D electrical properties as the thickness of the materials is less than ~20 nm and the surface of the materials is near atomically flat.

Very recently, the 2D electron system formed in the interface between MgZnO and ZnO is created and physics of fractional quantum Hall effect in ZnO is explored [17]. Alternatively, the 2D nature can be investigated in the 2D structure of ZnO. Cao et al. [18] adopted seed-layer assisted electrochemical route to synthesize ZnO platelets with tens of nanometers in thickness. The growth direction is along <01-10> within (0001) planes. Kaneti et al. [19] employed a hydrothermal method to make nanoflakes with thickness ranging from 20 to 35 nm whereas the exposed top surface is the (10-10) plane. The 2D structures of ZnO like nanosheets and nanoflakes are synthesized but the electron system whether reveals 2D nature or not is not studied

yet. Here a sequential hydrothermal process is used to synthesize ZnO nanoflakes and the electron system in the 2D structure is investigated.

ZnO nanoflakes were made by using a sequential hydrothermal process. A description of the synthesis method is given as follows. First, 10 g of zinc acetate dihydrate was dissolved at 60 °C in ethylene glycol methyl ether with ethanolamine equimolar of zinc acetate dehydrate under vigorous stirring for 30 min to form ZnO colloid. The colloid was subsequently spin-coated on a Si substrate as a seed layer. After coating Si substrate by the ZnO seed layer, the 1st-step hydrothermal growth of ZnO nanostructures was performed by suspending the substrate upside-down into a Teflon container filled with an equimolar aqueous solution (25 mM) of zinc nitrate ($Zn(NO_3)_2 \cdot 6H_2O$) and hexamethylenetetramine (HMTA, $(CH_2)_6N_4$). The growth temperature and time were set at 90 °C and 3 h, respectively. At the end of the growth, the sample substrate was removed from the solution, then rinsed with deionized water to remove any residual salt from the sample surface. The sample substrate was dried at 100 °C overnight. For the 2nd-step hydrothermal growth, the sample was placed in a solution with an equimolar aqueous solution (50 mM) of metal nitrate (zinc nitrate and cupper nitrate with equimolar) and HMTA. The hydrothermal reaction was carried out at 160-200 °C for 4-8 h. After the growth process, the sample was dried and annealed at 250 °C in vacuum for 24 h.

The morphology of as-synthesized ZnO nanoflakes was characterized using a transmission electron microscope (TEM, JEOL JEM-ARM200F), operated at an acceleration voltage of 200 kV, and a field-emission scanning electron microscope (SEM, JEOL JSM-7001). The morphology of nanoflakes dispersed on Si wafers was inspected by an atomic force microscope (AFM, Seiko SPA-300HV). The compositional analysis was carried out by an energy dispersive X-ray spectroscope (EDX, Oxford INCA Energy), equipped with the TEM. The lattice structure characterization was done by an X-ray diffractometer (XRD, D/MAX-2550, Cu as target radiation source using Kα line and the wavelength λ of 0.15406 nm). For electrical characterizations, a pair of contact electrodes were patterned on top of ZnO nanoflakes using standard electron-beam lithography, followed by thermal evaporation of a Ti/Au films (20/100 nm in thickness). The separation between the pair electrodes was kept at a constant of 1 μm for all devices in this study. To reduce increase the conductance of ZnO, the devices were annealed at 550 °C for 24 hours in a high vacuum (< 10^{-5} Torr). The ZnO nanoflake devices were loaded into an insert cryostat to acquire temperature dependence of electrical behaviors. The temperature for all the measurements is ranging from 80 to 300 K.

Figure 1(a) presents a typical SEM image of ZnO nanoflakes with optical image shown in the inset. The lateral size of the nanoflakes is about few micrometers whereas the thickness is about tens of nanometers. The nanoflakes are randomly distributed without any preferred orientations. In contrast to previous results [18,19], the sequential hydrothermal process produces considerably thinner ZnO nanoflakes. The AFM image as a complementary evidence is shown in Fig. 1(b). A line

profile of the ZnO nanoflake is given, as well, to show a thickness of 12 nm and sizes of 200-300 nm. The root-mean-square roughness of the surface is about 2.8 Å on an area of 100×100 nm^2. From the AFM measurements, the ZnO nanoflakes always show sharp and well-defined edges thus corroborating the crystallinity of the nanoflakes. The ultrathin nature of the nanoflakes benefits defect creation for improving conductivity in ZnO that will be discussed later. Figure 1(c) shows the EDX spectrum of the nanoflakes that indicates the presence of Zn and O elements in accompany with the C and Cu elements originating from the copper grid, and Fig. 1(d) presents the XRD spectra of nanoflakes post-annealed at 250 and 320 ^{o}C. The wurtzite structure of ZnO nanoflakes is evident and the sharp XRD peaks indicate a high degree of crystallinity. In addition, almost no impurities, reactants, or other secondary phases are detected within the resolution limit. The prominent peaks in Fig. 1(d) precisely correspond to the ZnO crystals (JCPDS 36-1451). The lattice spacing of the (002) planes is estimated to be 2.61 Å, leading to the *c* lattice constant of 5.22 Å. Unlike usual preferred growth in the <0001> direction for one-dimensional ZnO nanowires, the 2D ZnO structures have the strongest diffraction peak in the (101) or (100) plane. More particularly, Fig. 1(d) implies that a high post-annealing temperature of 320 ^{o}C results in an obviously decreased signal of the <001>, *c*-axis direction in comparison with that of the nanoflakes post-annealed at 250 ^{o}C.

Figure 2(a) presents TEM image of the ZnO nanoflakes. The size of the nanoflakes in the TEM image is 200-300 nm. It is very difficult to take TEM images. The ZnO nanoflakes usually melt during the time that the TEM images are taken since the nanoflakes are very thin. High-resolution TEM images of two different zone axes are shown in Figs. 2(b) and 2(c). Figure 2(b) presents a highly ordered lattice image at the <0001> zone axis and the lattice spacing of the $(10\bar{1}0)$ planes is 2.8 Å. It implies that the growth of the ZnO nanoflakes is along the $< 10\bar{1}0 >$ which is observed in Ref. 18. On the other hand, Fig. 2(c) presents another highly ordered lattice image at the $< 2\bar{1}\bar{1}0 >$ zone axis. The lattice spacing of (0002) planes is measured to be 2.6 Å which is almost the same as that evaluated from the XRD spectra. The result indicates another growth direction along the <0001> which is in agreement with that reported in Ref. 19. As a consequence, there are two different growth directions for the nanoflake formation. Before we make devices, the ZnO nanoflakes are dispersed on a Si wafer. AFM images are taken so as to give the statistical results of the thickness of the ZnO nanoflakes (see Fig. 2(d)). The average thickness and its standard deviation are ~17 and ~3.3 nm, respectively. These ZnO nanoflakes which are quite uniform in thickness are used for the following device making and electron transport measurements.

ZnO nanoflake devices, as shown in the inset to Fig. 3(a), are fabricated for the study of conduction mechanism at mesoscopic scales. The as-fabricated devices exhibit a resistance higher than 10^{10} Ω (Fig. 3(a)) at room temperature (RT). The ultrathin nature (thickness less than 20 nm) of the ZnO nanoflakes benefits the creation of oxygen vacancies in the thermal annealing process for reducing their electrical resistivity [20]. After a long period of thermal treatment, the RT resistance largely

drops by at least three orders of magnitude and its average value approaches ~5.5 × 10^6 Ω, also shown in Fig. 3(a). Current-voltage (I_{ds}-V_{ds}) characteristics of the ZnO nanoflake device (ZnO-1), expressed at various temperatures, are displayed in Figure 3(b). At a given source-drain current (I_{ds}), the source-drain voltage (V_{ds}) of the ZnO-1 device increases with decreasing temperature that suggests a semiconducting demeanor of electron transport. The linear dependence of the I_{ds}-V_{ds} curves implies the formation of Ohmic contact between the ZnO nanoflake and the Ti/Au electrodes so as to assure the intrinsic properties acquired from our electrical exploration. The RT resistivity of the ZnO-1 device is estimated to be about 25 Ω cm. Further, temperature dependent behaviors of three different nanoflake devices (ZnO-1 - ZnO-3) are investigated and displayed in Figure 3(c) where the resistivity is normalized by dividing with its RT value. The normalized resistivity of the devices increases with decreasing temperature and the resistivity in logarithmic scale manifest themselves as a linear dependence on $T^{-1/3}$ in a wide temperature range. The result reveals a strong indication of electron transport in ZnO nanoflakes that is in high compliance with the model of Mott's 2D variable-range hopping (2D VRH). According to the 2D VRH theory in which the temperature dependent resistivity $\rho(T)$ is expressed by the mathematical equation $(T) = \rho_0 \exp\left[(T_0/T)^{-1/3}\right]$ [21], the average values of the parameters ρ_0 and T_0, derived from the best fitting to all the data, are 2.83 × 10^{-4} Ω cm and 2.26 × 10^5 K, respectively.

To verify the fitting by the 2D VRH model for electron transport in the ZnO nanoflakes, I_{ds}-V_{ds} measurements under high electric fields were carried out and analyzed as follows. The 2D VRH model predicts high-field I_{ds}-V_{ds} following the equation $I = I_0 \exp\left[(k_B T_0 x/q\xi V_{ds})^{-1/3} \right]$ [21], where I_0, k_B, x, q, and ξ are weak electric-field dependent parameter, the Boltzmann constant, channel separation, elementary charge, and localization length of carriers, respectively. In the inset of Figure 3(c), the I_{ds}-V_{ds} data of the ZnO-1 device at 80 K are expressed in the form of ln(I_{ds}) versus $V_{ds}^{-1/3}$ and it precisely fits to the prediction of the 2D VRH model. From the best fit of data in the high-field regime (marked by a red solid line in the inset to Fig. 3(c)), the value of the localization length ξ is evaluated to be about 7 nm which is comparable with the thickness of the ZnO nanoflakes, supporting the comprehension of 2D transport mechanism as well as the hopping condition in such low-dimensional systems. Moreover, in the hopping transport mechanism, the average hopping energy W_{2D-VRH} and the most probable hopping distance R_{2D-VRH} can be extracted from the mathematical forms of $W_{2D-VRH} = (k_B T/3)(T_0/T)^{1/3}$ and $R_{2D-VRH} = (\xi/3)(T_0/T)^{1/3}$ [21]. Temperature dependence of hopping energy (the left panel) and hopping distance (the right panel) of electrons in the ZnO nanoflakes are plotted in Figure 3(d). The hopping energy W_{2D-VRH} and hopping distance R_{2D-VRH} are estimated to be 78.4 meV and 21.2 nm at RT. The hopping energy W_{2D-VRH} and hopping distance R_{2D-VRH} at all temperatures lower than 300 K strictly satisfy the criteria of hopping energy higher than thermal energy ($W_{2D-VRH} > k_B T$) and hopping

distance longer than localization length ($R_{2D-VRH} > \xi$) as required conditions for VRH. The result offers again a strong evidence of 2D transport for carriers in the nanoflakes.

For an application of 2D semiconductors like ZnO nanoflakes, the electron transport in the 2D system needs to be characterized thoroughly. Here the sequential hydrothermal process is used to make ZnO nanoflakes. The morphology of 2D structures is inspected by SEM for as-synthesized nanoflakes, and confirmed again by AFM for dispersed samples on the Si wafer. The average thickness is ~17 nm. The EDX and XRD spectra present that no impurities and secondary phases in ZnO nanoflakes and, furthermore, the high-resolution TEM images show two possible growth directions along the $< 10\bar{1}0 >$ and the $< 0001 >$. Two-probe electrodes are made on ZnO nanoflakes for electrical characterizations. Due to the ultrathin nature of the nanoflakes, the resistivity is decreased to ~25 Ω cm after a long period of thermal annealing in a high vacuum. The temperature and electric field dependences precisely follow the prediction of Mott's 2D VRH theory thus the localization length of ~7 nm is determined. The hopping energy and the hopping distance of electrons in ZnO nanoflakes are evaluated as a function of temperature. The estimated quantities all confirm the 2D property of electrons in the system thus supporting the application of ZnO nanoflakes as a 2D channel in electronic devices.

ACKNOWLEDGEMENT

This work was supported partially by the NSFC(TBF), the National Science and Technology project of Guangdong Province (2014KTSCX108 (DLJ)), Shenzhen Science and Technology project (JCYJ20150525092940969 (DLJ), JCYJ20150525092941038 (JPZh), JCYJ20140428091413577 (ILL) and JCYJ20130329103213543 (PH)). This work was also supported by the Taiwan Ministry of Science and Technology under Grant Number MOST 104-2119-M-009-009-MY3 and MOST 103-2628-M-009-004-MY3.

REFERENCES

1. C. Klingshirn, ChemPhysChem **8**, 782 (2007).
2. H. Frohlich and N. F. Mott, Proc. Roy. Soc. (London), Ser. A **171**, 496 (1939).
3. D. G. Thomas1 and J. J. Lander, J. Chem. Phys. **25**, 1136 (1956).
4. D. C. Look, J. Electron. Mater. **35**, 1299 (2006).
5. Ü. Özgür, Ya. I. Alivov, C. Liu, A. Teke, M. A. Reshchikov, S. Doğan, V. Avrutin, S.-J. Cho, H. Morkoç, J. App. Phy. **98**, 041301 (2005).
6. Yong-Sung Kim and C. H. Park, Phys. Rev. Lett. **102**, 086403 (2009).
7. D. C. Look and B. Claflin, Phys. Stat. Sol. b **241**, 624 (2004).
8. D. M. Bagnall, Y. F. Chen, Z. Zhu, T. Yao, S. Koyama, M. Y. Shen and T. Goto, Appl. Phys. Lett. **70**, 2230 (1997).
9. M. H. Huang, Y. Wu, H. Feick, N. Tran, E. Weber, and P. Yang, Adv. Mater. 13, 113 (2001).

10. Z. L. Wang, J. Phys. Chem. B **104**, 1153 (2000).
11. J. G. Lu, P. Chang, and Z. Fan, Mater. Sci. Eng. R **52**, 49 (2006).
12. Y. Qin, X. Wang, and Z. L. Wang, Nature **451**, 809 (2008).
13. L. Jin and L. Li, Nano Energy **15**, 776 (2015).
14. K. S. Novoselov, A. K. Geim, S. V. Morozov, D. Jiang, Y. Zhang, S. V. Dubonos, I. V. Grigorieva, and A. A. Firsov, Science **306**, 666 (2004).
15. S. Z. Butler et al., ACS Nano **7**, 2898 (2013).
16. S. V. Kravchenko and M. P. Sarachik, Rep. Prog. Phys. 67, 1 (2004).
17. J. Falson, D. Maryenko, B. Friess, D. Zhang, Y. Kozuka, A. Tsukazaki, J. H. Smet, and M. Kawasaki, Nature Physics **11**, 347 (2015).
18. B. Cao, X. Teng, S. H. Heo, Y. Li, S. O. Cho, G. Li, and W. Cai, J. Phys. Chem. C **111**, 2470 (2007).
19. Y. V. Kaneti, J. Yue, X. Jiang, and A. Yu, J. Phys. Chem. C **117**, 13153 (2013).
20. Jin Liu, Puxian Gao, Wenjie Mai, Changshi Lao, Zhong L. Wang, and Rao Tummal, Appl. Phys. Lett. **89**, 063125 (2006).
21. D. Shahar and Z. Ovadyahu, Phys. Rev. Lett. **64**, 2293 (1990)

FIGURE CAPTION

FIG. 1. (a) SEM image of as-grown ZnO nanoflakes with a scale bar of 1 μm. The inset gives an optical image of ZnO nanoflakes on Si wafers. (b) AFM image of ZnO nanoflakes on Si wafer with a marked line and its line profile information. (c) TEM EDX spectrum of identified Zn, O, Cu, and C elements. (d) XRD patterns marked with identified lattice planes of ZnO for ZnO nanoflakes post-annealed at two different temperatures.

FIG. 2. (a) TEM image of ZnO nanoflakes. (b), (c) The high-resolution TEM image shows the atomic structure with zone axis, lattice plane, and spacing marked on it. (d) Statistical distribution of the thickness of ZnO nanoflakes that is estimated from AFM images. The average thickness is ~17 nm and the standard deviation is ~3.3 nm.

FIG. 3. (a) Histogram of RT resistances of ZnO nanoflake devices with or without thermal annealing. SEM image of a typical ZnO nanoflake device is shown in the inset. (b) I_{ds}-V_{ds} curves of the ZnO nanflake (ZnO-1) device at various temperatures. (c) Resistivity as a function of temperature for three devices. The resistivity is divided by its RT value for comparison. The solid lines present the best fits to data. The inset shows the I_{ds}-V_{ds} of the ZnO-1 in the form of $\ln(I_{ds})$-$V_{ds}^{-1/3}$. The solid line indicates the high-field approaching manner. (d) Hopping energy and hopping distance as a function of temperature. The dashed line demonstrates thermal energy for comparison.

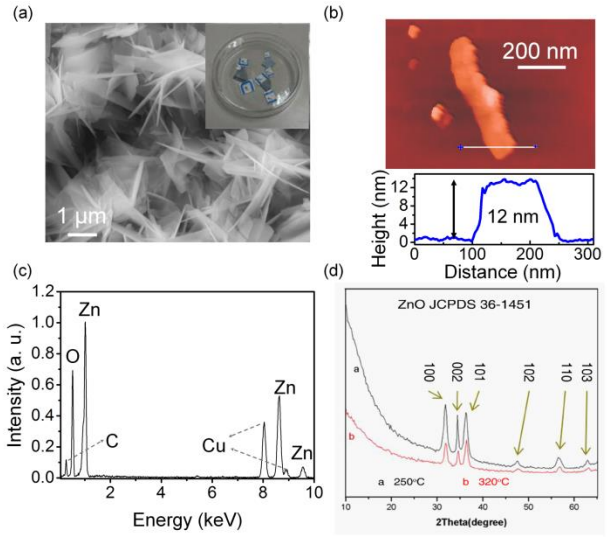

FIG. 1. (a) SEM image of as-grown ZnO nanoflakes with a scale bar of 1 μm. The inset gives an optical image of ZnO nanoflakes on Si wafers. (b) AFM image of ZnO nanoflakes on Si wafer with a marked line and its line profile information. (c) TEM EDX spectrum of identified Zn, O, Cu, and C elements. (d) XRD patterns marked with identified lattice planes of ZnO for ZnO nanoflakes post-annealed at two different temperatures.

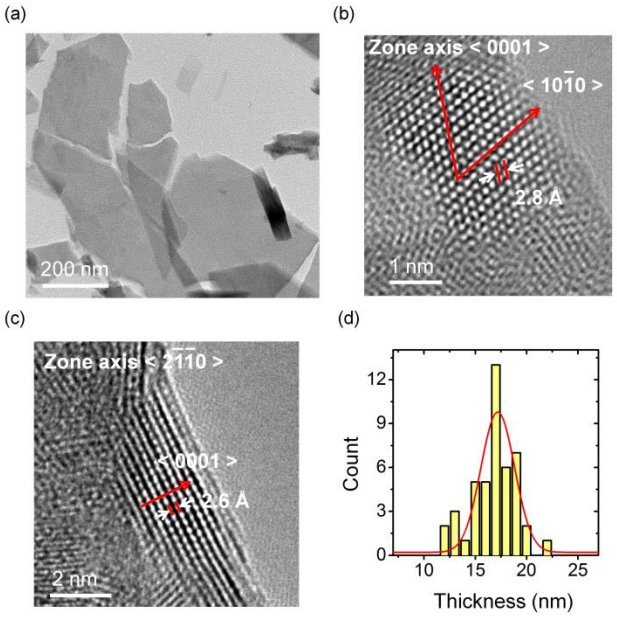

FIG. 2. (a) TEM image of ZnO nanoflakes. (b), (c) The high-resolution TEM image shows the atomic structure with zone axis, lattice plane, and spacing marked on it. (d) Statistical distribution of the thickness of ZnO nanoflakes that is estimated from AFM images. The average thickness is ~17 nm and the standard deviation is ~3.3 nm.

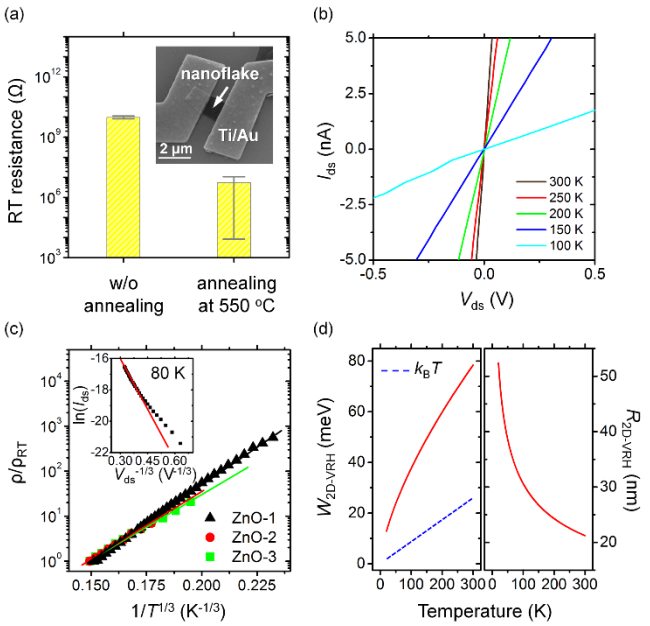

FIG. 3. (a) Histogram of RT resistances of ZnO nanoflake devices with or without thermal annealing. SEM image of a typical ZnO nanoflake device is shown in the inset. (b) I_{ds}-V_{ds} curves of the ZnO nanflake (ZnO-1) device at various temperatures. (c) Resistivity as a function of temperature for three devices. The resistivity is divided by its RT value for comparison. The solid lines present the best fits to data. The inset shows the I_{ds}-V_{ds} of the ZnO-1 in the form of ln(I_{ds})-$V_{ds}^{-1/3}$. The solid line indicates the high-field approaching manner. (d) Hopping energy and hopping distance as a function of temperature. The dashed line demonstrates thermal energy for comparison.